INTEGRATING UAV-DERIVED VARI, GNDVI, NDVI, AND NDRE FOR PHENOLOGICAL RICE GROWTH ANALYSIS

Asmala Ahmad[1,2], Mohd Yazid Abu Sari[3], Mohd Nasran Hasan[4], Wan Mohd Yaakob Wan Bejuri[1,2], Hamzah Sakidin[5], Suliadi Firdaus Sufahani[6], Abd Rahman Mat Amin[7] and Abd Wahid Rasib[8]
[1]OptiMAS Research Group, Centre for Advanced Computing Technology (C-ACT), Faculty of Information and Communication Technology, Universiti Teknikal Malaysia Melaka, Durian Tunggal, Melaka, Malaysia
[2]Faculty of Artificial Intelligence and Cyber Security, Universiti Teknikal Malaysia Melaka, Melaka, Malaysia
[3]Anjung Technology Sdn. Bhd., Ayer Keroh, Melaka, Malaysia
[4]Perbadanan Melaka (MCORP), Kompleks MITC, Ayer Keroh, Melaka
[5]Department of Fundamental and Applied Sciences, Universiti Teknologi PETRONAS, Perak, Malaysia
[6]Fakulti Sains Gunaan dan Teknologi, Universiti Tun Hussein Onn Malaysia, Parit Raja, Batu Pahat, Johor, Malaysia
[7]Fakulti Sains Gunaan, Universiti Teknologi MARA Cawangan Terengganu, Kuala Terengganu, Terengganu, Malaysia
[8]Fakulti Alam Bina Dan Ukur, Universiti Teknologi Malaysia, UTM Skudai, Johor, Malaysia
E-Mail: asmala@utem.edu.my

ABSTRACT

This study investigates the effectiveness of UAV-based multispectral vegetation indices, namely Visible Atmospherically Resistant Index (VARI), Green Normalized Difference Vegetation Index (GNDVI), Normalized Difference Vegetation Index (NDVI), and Normalized Difference Red Edge (NDRE) for temporal and spatial monitoring of rice crop growth over a 117-day cultivation period. UAV imagery was collected at nine key growth stages and processed to derive the indices. Quantitative analysis revealed that NDVI, GNDVI, and VARI were highly correlated ($r = 0.77$-0.93), reflecting strong sensitivity to canopy greenness and chlorophyll content, whereas NDRE exhibited low correlation with the other indices ($r = -0.20$ to 0.01), indicating its complementary role in detecting subtle physiological changes during reproductive and ripening phases. These findings demonstrate that integrating multiple indices enhances phenological monitoring, offering a robust, high-resolution, and cost-effective approach for precision rice agriculture.

Keywords: vegetation indices, UAV, rice, remote sensing, precision agriculture.

Manuscript Received 23 August 2025; Revised 10 December 2025; Published 30 December 2025

INTRODUCTION

Rice is a staple food for over three billion people worldwide, around 50% of the world population [1] [2]. It is a key component of food security in many countries. Although the world's rice cultivation area is growing exponentially, the total demand for rice has always exceeded production. The area of rice farming land is approximately 12% of the world's total agricultural land, with an area of 167.3 million hectares [3]. Rice production around the world is still unable to meet the current demand due to the suboptimal rice harvest. This situation is caused by several factors, such as poor management, natural disasters, disease outbreaks, and weather changes. Thorough continuous monitoring is essential for identifying the causes of the decrease in rice harvesting that eventually leads to a decline in rice productivity. Rice crop requires suitable conditions to grow, which include topography, soil, weather, and irrigation system. However, rice sustainability can be disrupted at any time due to various factors including crop disease outbreaks, global climate change, instability in bilateral relation between countries, economic crisis, and war [5].

The main challenges for rice production are the decrease in rice crop area due to urbanisation, ageing farmers, high cost of rice production, irrigation efficiency, and lack of systematic practices in managing rice crops, particularly on a larger scale [6]. In monitoring health conditions of rice crops, farmers practice the traditional eye observation approach via ground scouting. Such an approach is exposed to human errors, time-consuming, and unable to provide information on the rice crop effectively. Managers and farmers only get to know the true conditions of the crops at the end of the season, after harvesting is done. If the yield is unsatisfactory, then the managers and farmers start to look for possible reasons to improve during the following new season. Such practices cause unnecessary cost to managers and farmers, and in the end not result in an optimal crop yield.

Efforts to resolve such issues have been carried out in many parts of the world through various means [7] [8] [9] [10] [11] [12] to ensure global food security. Precision agriculture has been found to be a promising solution [13] [14] [15] and can be defined as a method to improve the effectiveness of agricultural management. Precision agriculture also refers to systems and methods of holistically managing crops by optimizing the use of resources [16] [17] with the right input, at the right time, and in the right location to maximize yield. This is also known as a '3R' concept in agriculture. In doing so, remote sensing technology is often used to monitor plant status

ARPN Journal of Engineering and Applied Sciences

[18] [19] [20]. Remote sensing technology has long been beneficial for this purpose because of its ability to record images continuously and at a cheaper cost [21].

Remote sensing technology based on satellite platforms has been widely used for rice crop monitoring in many parts of the world, particularly for applications such as crop classification, crop monitoring, and yield estimation. However, satellite remote sensing faces inherent limitations in spatial and temporal resolution [22] [23]. The temporal resolution of most satellite imagery is constrained by revisit cycles of several days to weeks, which may not be sufficient for capturing the rapid changes in rice growth that occur within short intervals. In addition, the spatial resolution of many satellite sensors is typically at the meter scale; therefore, it is often inadequate for rice monitoring, given the relatively small physical structure of rice plants. As an alternative, UAV-based remote sensing offers significantly higher spatial and temporal resolution, along with the flexibility to customize spectral configurations. These advantages make UAV platforms particularly well-suited for precise, timely, and detailed rice crop monitoring.

Rice Growth Stages

Rice growth is fundamentally dependent on photosynthetic activity, which is essential for generating the energy and biomass required for development, making it a vital process to monitor. Photosynthesis involves the conversion of carbon dioxide and water into glucose and oxygen in the presence of light energy, particularly within the wavelength range of 680–700 nm. The growth cycle of rice typically spans from day 0 to day 120. Monitoring changes in the spatial and spectral properties of the crop throughout this period provides critical information for identifying and characterizing the different growth stages of rice [11].

Figure-1 illustrates the phenological timeline of transplanted rice, detailing the progression from field preparation to harvest. The growth cycle is divided into three main phases: Vegetative, Reproductive, and Ripening. Following a nursery stage of approximately 20-25 days, seedlings enter the Vegetative Phase, which spans 36-76 days depending on cultivar maturity class (short-, medium-, or long-duration). This phase encompasses early tillering, canopy expansion, and stem elongation. The Reproductive Phase, lasting about 35 days, begins with panicle initiation and continues through booting, heading, and flowering, during which reproductive structures develop, and grain set occurs. The final Ripening Phase (~30 days) involves grain filling, maturation, and physiological readiness for harvest. Total crop duration ranges from 100-120 days for short-duration varieties, 120-140 days for medium-duration varieties, and 140-160 days for long-duration varieties.

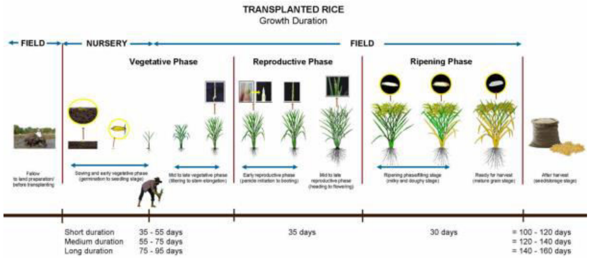

Figure-1. Rice growth stages [11].

Vegetation Indices

Vegetation indices derived from remote sensing have been widely recognized as effective indicators for assessing plant growth dynamics. These indices are calculated from the electromagnetic reflectance captured from the plant canopy using passive optical sensors. The spectral reflectance of vegetation is strongly influenced by both chemical and morphological properties of plant tissues, such as leaf pigments, water content, and structural characteristics. It also varies according to plant species and intrinsic physiological conditions. With advancements in sensor technology offering high spectral resolution, numerous vegetation indices have been developed in previous studies to quantify crop vigor, photosynthetic activity, and overall plant health [6]. Since individual measurement of spectral reflectance (R) at different wavelengths (λ) has a unique capability, several vegetation indices can be generated by making use of different R_λ as follows:

a) Visible Atmospherically Resistant Index (VARI) is a vegetation index that takes advantage of the green (R_{550nm}), red (R_{670nm}), and blue (R_{450nm}) bands to minimize the influence of atmospheric effects in the visible spectrum and assess vegetation health. VARI is particularly effective in enhancing vegetation information under conditions of strong atmospheric disturbance and in reducing the impact of illumination variations, thereby providing more reliable vegetation assessment [6]:

$$\mathrm{VARI} = \frac{(R_{550nm} - R_{670nm})}{(R_{550nm} + R_{670nm} - R_{450nm})} \quad (1)$$

VARI values range from -1 to +1. Values below 0 generally correspond to non-vegetated surfaces such as soil or water; values near 0 indicate sparse or low vegetation cover, while positive values represent increasing levels of vegetation greenness and vigor, with higher values reflecting healthier and denser vegetation.

b) Normalized Difference Vegetation Index (NDVI) is one of the most widely used vegetation indices, calculated using reflectance from the red (R_{670nm}) and near-infrared (R_{800nm}) spectral bands. NDVI provides valuable insights into plant vigor, chlorophyll content, and above-ground biomass by exploiting the strong absorption of red light by chlorophyll and the high

ARPN Journal of Engineering and Applied Sciences

reflectance of near-infrared light by healthy plant cell structures. NDVI formula can be expressed as follows [24]:

$$NDVI = \frac{(R_{800nm} - R_{670nm})}{(R_{800nm} + R_{670nm})} \quad (2)$$

NDVI values range from -1 to +1. Values approaching +1 represent healthy, dense vegetation with high chlorophyll activity, values near 0 correspond to sparse vegetation or bare soil, while negative values generally indicate water bodies, built-up areas, or other non-vegetated surfaces.

c) Green Normalized Difference Vegetation Index (GNDVI) evaluates crop health and photosynthetic activity by utilizing reflectance from the green (R_{550nm}) and near-infrared (R_{800nm}) spectral bands. GNDVI is particularly sensitive to chlorophyll concentration and canopy structure, making it effective for monitoring plant vigor, nitrogen status, and early stress detection [25][26]. The GNDVI formula is given as follows:

$$GNDVI = \frac{(R_{800nm} - R_{550nm})}{(R_{800nm} + R_{550nm})} \quad (3)$$

GNDVI values range from -1 to +1. Negative values (<0) generally correspond to bare soil, water, or other non-vegetated surfaces. Values near 0 indicate sparse vegetation with low chlorophyll content, while positive values reflect increasing vegetation density, chlorophyll concentration, and overall plant health.

d) Normalized Difference Red Edge Index (NDRE) NDRE is a vegetation index that combines reflectance from the red-edge region (R_{720nm}) and the near-infrared (R_{800nm}) band. It is highly sensitive to subtle changes in plant health, particularly related to chlorophyll content and canopy structure. NDRE is especially effective for monitoring crop nitrogen status, detecting early stress conditions, and assessing vegetation in later growth stages when traditional indices such as NDVI may become saturated [25][26]. The higher the NDRE value, the greater the chlorophyll content in the leaves, indicating healthier and more vigorous vegetation. NDRE is calculated using the following formula:

$$NDRE = \frac{(R_{800nm} - R_{720nm})}{(R_{800nm} + R_{720nm})} \quad (4)$$

NDRE values range from -1 to +1. Values approaching +1 indicate healthy vegetation with high chlorophyll content and strong photosynthetic activity, while values near 0 reflect sparse or stressed vegetation. Negative values are generally associated with non-vegetated surfaces such as water, bare soil, or built-up areas.

METHODOLOGY

Image acquisition was carried out based on the Personal Remote Sensing System or PRSS concept [10]. The PRSS concept has been established for overcoming limitations in terms of spatial resolution, besides cloud and haze effects that degrade space-borne remote sensing satellite imagery [27][28][29]. This system consists of 1) an aerial segment, 2) a ground segment, and 3) a user segment. The aerial segment consists of a quadrotor UAV that is equipped with GPS and telemetry facilities and mounted with a high-resolution RGB camera [10]. Images are captured automatically at desired time intervals and stored in the camera's storage card. Upon completing an image acquisition mission, images in the card are transferred to the ground segment for subsequent image processing tasks. The ground segment consists of a laptop installed with software for controlling and tracking the UAV, besides processing captured images. Processed images are finally uploaded to the cloud-based geospatial databases that can be accessed and personalised using a smartphone in the user segment. Figure-2 (a) illustrates the PRSS concept.

In this study, the study area was Kampung Sawah Sagil, located in Batu Pahat, Johor, Malaysia, with an area of approximately 70 ha (0.7 km^2). The UAV was flown at a height of 66 m, giving a ground sampling distance (GSD) of 1.43 cm. Image acquisitions were set for the three phases of rice growth, namely vegetative, reproductive, and ripening. For each phase, image acquisitions were performed three times to represent nine series of rice growth from day 0 to day 117. Figure-2 (b) shows the flowchart for this study. For a single image acquisition mission, about 2,100 images were captured and stitched. RGB images were used to generate an orthophotography of the study area. Figure-3 shows the pre-set pathways of the UAV over the study area. The multispectral image we used to produce a vegetation index image of the study area for VARI, GNDVI, NDVI, and NDRE.

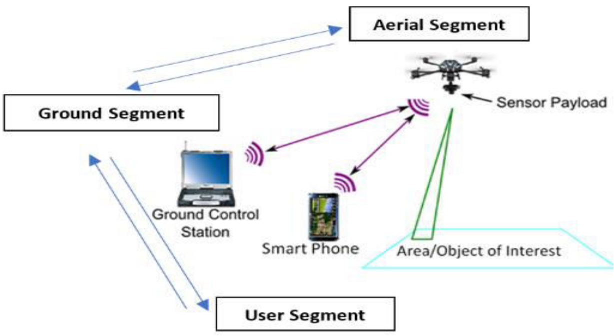

(a)

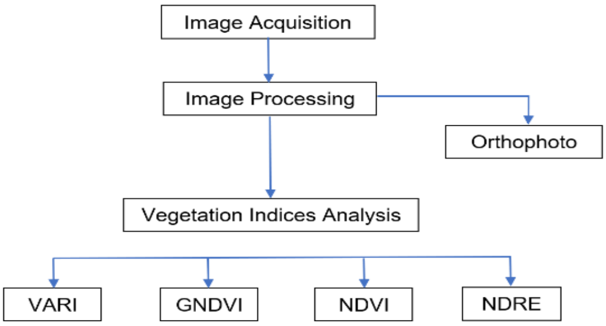

(b)

Figure-2. (a) The PRSS concept and (b) the study flowchart.

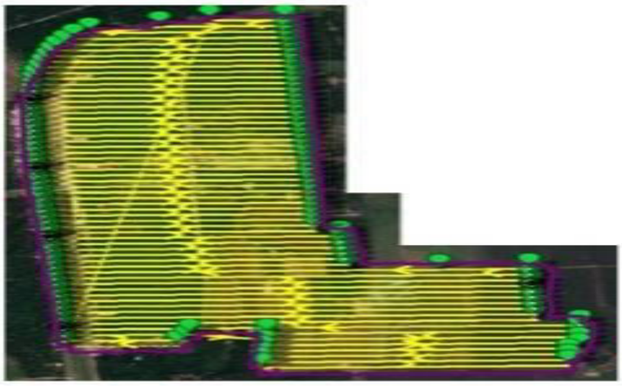

Figure-3. The pre-set pathways for the image acquisition mission over the rice field.

RESULTS AND DISCUSSIONS

Figure-4 shows the study area displayed as (a) an RGB orthophoto and (b) the digital elevation model (DEM) of the study area. From the RGB orthophoto, it is obvious that rice crops dominate the area, surrounded by other vegetation types such as oil palms and other crops. The RGB orthophoto reveals that the landscape is predominantly covered by rice crops, interspersed with other vegetation such as oil palms and cash crops. The DEM illustrates the ground surface elevation, where the color gradient ranges from 0 meters (blue) to 29 meters (red). The terrain is generally flat, with most areas having an elevation between 5 and 10 meters, and is suitable for rice cultivation due to uniform water distribution and efficient irrigation. Figure-4 (c) shows orthophoto images on day 9, day 23, day 37, day 56, day 67, day 76, day 95, day 106, and day 117. During the early vegetative phase (Day 9 to Day 37), the images appear predominantly brown and grey, indicating exposed soil and minimal plant canopy. These tones reflect the early stages of seedling development, where rice plants are sparse, small, and have not yet formed a continuous leaf cover. From Day 56 to Day 76, corresponding to the reproductive phase, the imagery becomes significantly greener. This colour shift reflects vigorous vegetative growth, as the rice plants develop more leaves and reach their peak photosynthetic capacity. The increasing density of green pixels indicates a healthier, more uniform canopy, typical of panicle initiation and flowering. By Day 95 through Day 117, during the ripening phase, the field displays a mosaic of green and yellow tones. This colour change marks the physiological maturity of the rice plants, as chlorophyll content declines and the grains begin to harden and turn golden.

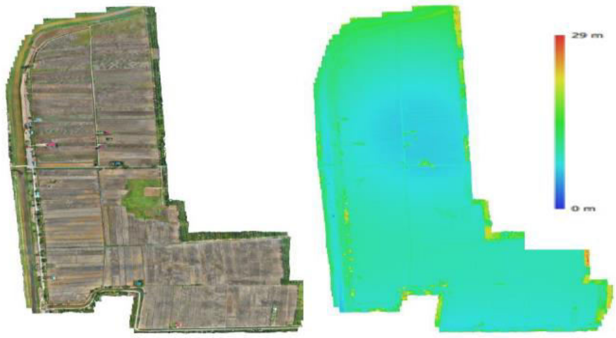

(a) (b)

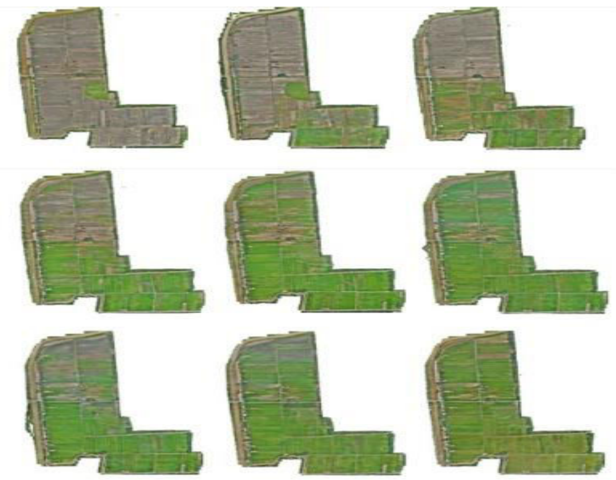

(c)

Figure-4. (a) RGB Orthophoto, (b) DEM of the study area, and (c) Orthophoto images (top) day 9, day 23, day 37, (middle) day 56, day 67, day 76, and (bottom) day 95 day 106 and day 117.

ISSN 1819-6608
ARPN Journal of Engineering and Applied Sciences

RGB Analysis

For further analyses, a plot with an area of 0.8 ha was selected. The plot is chosen due to having comparatively less interplot variability and can be easily accessed by vehicle. Figure-5 (top) shows RGB images of the selected plot while the bottom images for (a) day 9, (b) day 23, (c) day 37, (d) day 56, (e) day 67, (f) day 76, (g) day 95, (h) day 106 and (i) day 117. It can be seen that during the vegetative phase, particularly on day 9 and day 23, watery soil can be seen within the plot, indicated by brownish colour. During day 37, rice crops start to have leaves, indicated by the greenish colour within the plot. During days 56, 67, and 76, rice crops within the plot have more leaves as indicated by the green colour within the plot, allowing photosynthesis activities to take place in the leaves. During days 95, 106, and 117, flowering, followed by grain filling, takes place as indicated by the yellowish colour within the plot. This visual progression across time highlights the effectiveness of UAV-based RGB imagery in monitoring phenological changes in rice crops at the plot level.

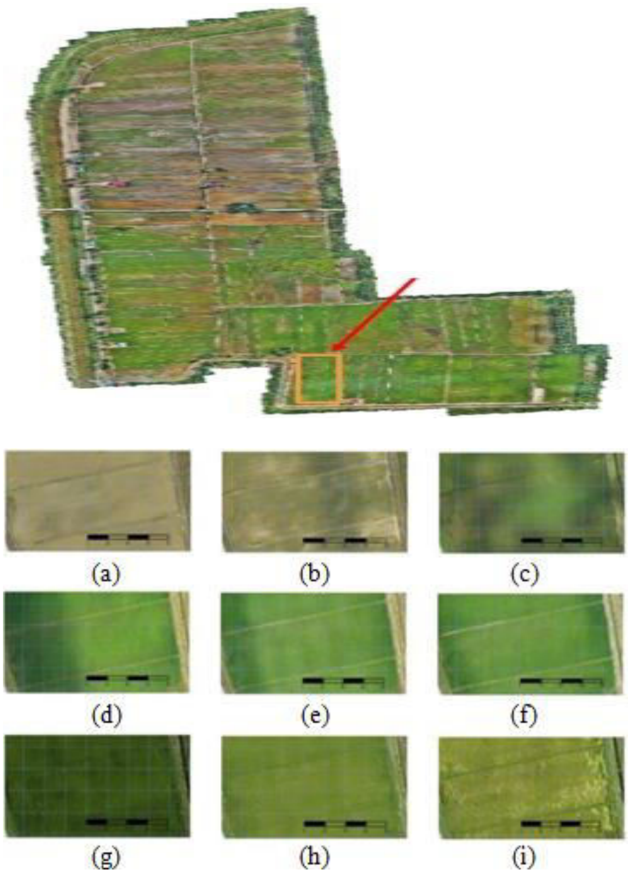

Figure-5. RGB images of the selected plot as indicated by the red arrow on the top image for (a) day 9, (b) day 23, (c) day 37, (d) day 56, (e) day 67, (f) day 76, (g) day 95, (h) day 106 and (i) day 117.

VARI Analysis

Figure-6 shows VARI images of the selected plot for (a) day 9, (b) day 23, (c) day 37, (d) day 56, (e) day 67, (f) day 76, (g) day 95, (h) day 106, and (i) day 117. The early-stage images (Days 9-37) show predominantly yellowish tones, corresponding to lower VARI values (0.23-0.28) due to sparse canopy coverage and higher soil background influence. From Day 56 onwards, the images transition to greener tones, reflecting increased canopy density and chlorophyll content, with VARI values rising steadily through the mid vegetative phase. The highest VARI (0.37) is observed on Day 95 during the reproductive stage, as shown in Figure-7, indicating peak vegetation vigor. A slight decline is noted in the ripening phase (Days 106–117) as the crop approaches maturity, consistent with physiological ripening.

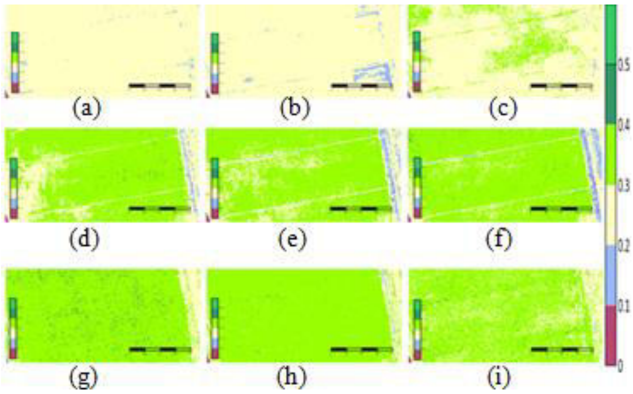

Figure-6. VARI images of the selected plot for (a) day 9, (b) day 23, (c) day 37, (d) day 56, (e) day 67, (f) day 76, (g) day 95, (h) day 106, and (i) day 117.

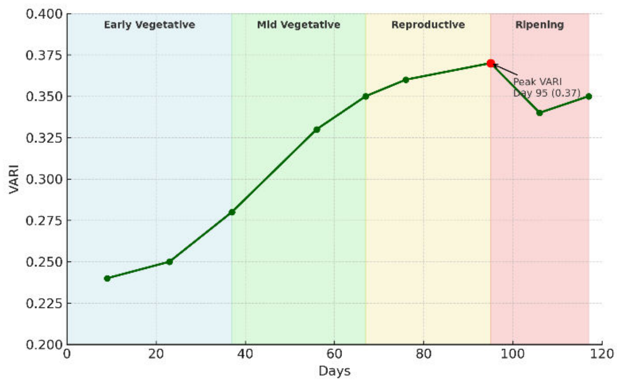

Figure-7. Time series average VARI of the selected plot from day 9 through day 117.

GNDVI Analysis

In Figure-8, early growth stages (Days 9-37) exhibit mixed yellowish and pinkish tones, corresponding to low or negative GNDVI values (-0.02 to -0.04), indicating sparse canopy cover and strong soil background influence. By Day 56, greener tones dominate, reflecting higher chlorophyll concentration and improved canopy density, with GNDVI rising to 0.20. This increase continues into the reproductive phase, reaching a peak of 0.26 on Day 95, as shown in Figure-9. The ripening phase (Days 106-117) is marked by a noticeable decline in

 ISSN 1819-6608
ARPN Journal of Engineering and Applied Sciences

GNDVI values (0.21 to 0.13), consistent with the onset of ripening and reduced photosynthetic activity. The temporal profile in Figure-9 shows a less uniform upward trend compared to VARI, with short-term fluctuations likely caused by variable leaf structure and spectral reflectance sensitivity in the green band.

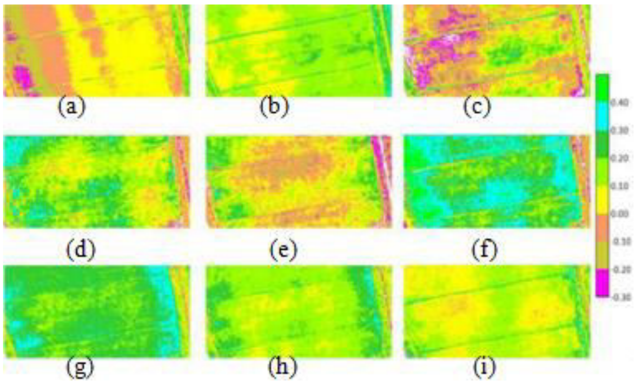

Figure-8. GNDVI images of the selected plot for (a) day 9, (b) day 23, (c) day 37, (d) day 56, (e) day 67, (f) day 76, (g) day 95, (h) day 106, and (i) day 117.

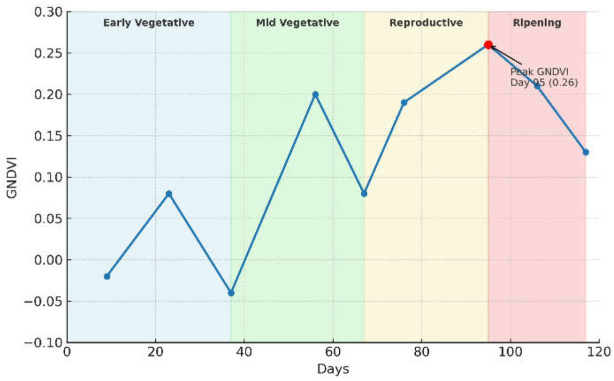

Figure-9. Time series average GNDVI of the selected plot from day 9 through day 117.

NDVI Analysis

In Figure-10, early growth stages (Days 9-37) are dominated by yellow to purple tones, representing low NDVI values (0.06-0.23) due to sparse canopy cover and significant soil background influence. From Day 56 onwards, greener tones become prevalent, with NDVI rising to 0.39 during the mid-vegetative phase, indicating vigorous canopy development and increased photosynthetic activity. As shown in Figure-11, NDVI continues to increase through the reproductive phase, peaking at 0.57 on Day 95, which corresponds to maximum biomass accumulation and optimal leaf area index. This peak marks the period of highest photosynthetic efficiency before the onset of ripening. During the ripening phase (Days 106-117), NDVI decreases to 0.34, reflecting chlorophyll degradation, leaf yellowing, and a reduction in canopy greenness as the crop approaches maturity. The consistent upward trend followed by a sharp decline demonstrates NDVI's strong sensitivity to structural and physiological changes across rice growth stages, making it a reliable indicator for phenological monitoring and yield forecasting.

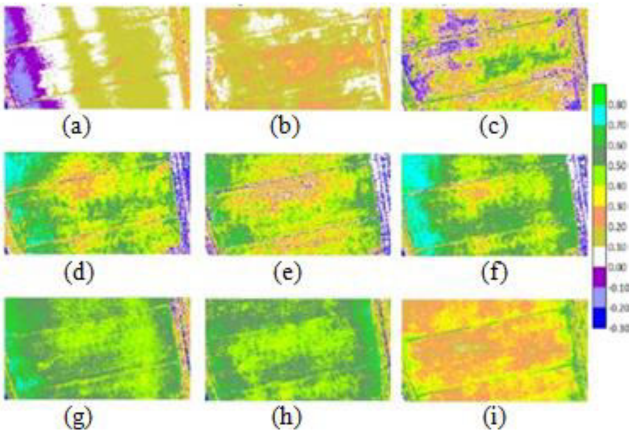

Figure-10. NDVI images of the selected plot for (a) day 9, (b) day 23, (c) day 37, (d) day 56, (e) day 67, (f) day 76, (g) day 95, (h) day 106 and (i) day 117Time series GNDVI of the selected plot from day 9 through day 117.

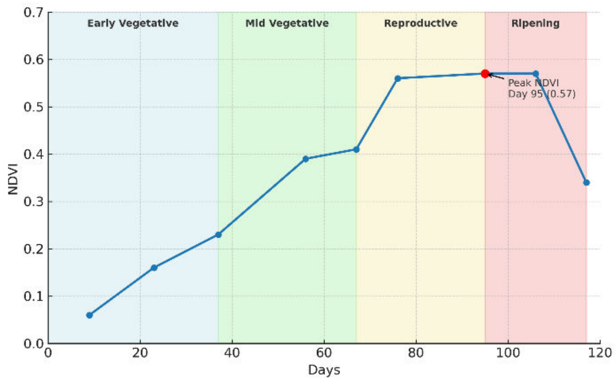

Figure-11. Time series average NDVI of the selected plot from day 9 through day 117.

NDRE Analysis

In Figure-12, the early vegetative stage (Days 9-37) is dominated by yellowish to purple tones, indicating low or negative NDRE values (-0.10 to 0.00). This reflects limited canopy density and minimal chlorophyll absorption in the red-edge region, as the plants are still in early growth with high soil background influence. By the mid vegetative phase (Days 56-76), isolated patches of green begin to appear, showing moderate NDRE values (~0.00 to 0.02), which correspond to increased chlorophyll concentration and canopy development. However, NDRE remains lower compared to other vegetation indices such as NDVI and GNDVI, indicating its heightened sensitivity to subtle chlorophyll changes rather than overall biomass.
As depicted in Figure-13, NDRE exhibits fluctuating values across the growing season, peaking at 0.05 on Day 106 during the ripening stage. This delayed peak relative

ARPN Journal of Engineering and Applied Sciences

to NDVI and VARI suggests that NDRE is more responsive to late-stage physiological changes, particularly variations in chlorophyll content and leaf pigment composition before ripening. The subsequent decline by Day 117 marks rapid chlorophyll degradation and loss of photosynthetic activity. This shows that NDRE provides complementary insight to other indices by highlighting red-edge reflectance shifts that occur during both the onset of maturity and ripening, making it a valuable tool for fine-scale monitoring of crop health and nutrient status during late growth phases.

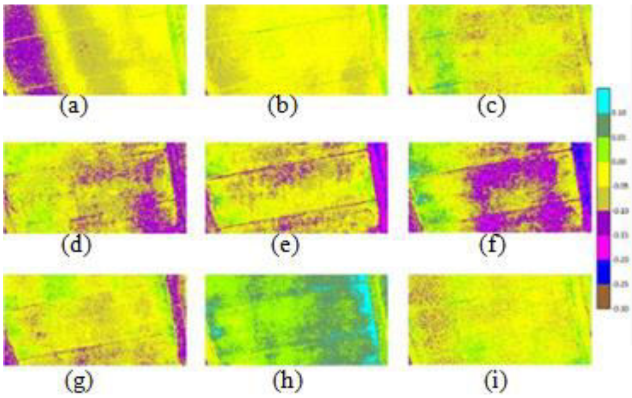

Figure-12. NDRE images of the selected plot for (a) day 9, (b) day 23, (c) day 37, (d) day 56, (e) day 67, (f) day 76, (g) day 95, (h) day 106, and (i) day 117.

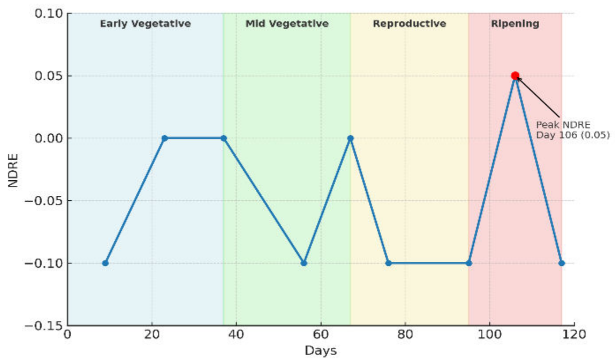

Figure-13. Time series average NDRE of the selected plot from day 9 through day 117.

Relationships among VARI, GNDVI, NDVI, and NDRE

Figure-14 (a) shows the temporal dynamics of four vegetation indices-VARI, GNDVI, NDVI, and NDRE-across the rice growth cycle from Day 9 to Day 117, with shaded backgrounds indicating the Early Vegetative, Mid Vegetative, Reproductive, and ripening phases. NDVI consistently records the highest values among the indices, increasing sharply from 0.23 at Day 37 to a peak of 0.57 during the reproductive phase (Days 95-106), reflecting maximum canopy greenness and chlorophyll density. GNDVI follows a similar pattern but with slightly lower magnitudes, peaking at 0.26 on Day 95, indicating a close association with photosynthetic activity but a reduced sensitivity to soil background effects. VARI, although starting with lower values (0.25 at Day 9), exhibits a steady increase until peaking at 0.37 on Day 95, highlighting its robustness under varying lighting conditions and soil influence. NDRE remains relatively low throughout the cycle, with values fluctuating around -0.10 to 0.05, but its slight positive shift during the reproductive stage suggests sensitivity to changes in leaf internal structure and pigment composition at later growth stages. Figure-14 (b) presents the correlation matrix between the four indices. Strong positive correlations are observed between NDVI and VARI (r ≈ 0.93), NDVI and GNDVI (r ≈ 0.88), and VARI and GNDVI (r ≈ 0.78), indicating that these indices track similar canopy development trends. NDRE, however, shows weak to negligible correlation with the other indices (r ranging from -0.20 to 0.15), implying it captures complementary information, particularly related to plant stress and late-stage physiological changes not detected by visible-spectrum indices. This divergence suggests that integrating NDRE with the other indices could improve the sensitivity of rice growth monitoring models, especially for detecting stress signals during the ripening phase.

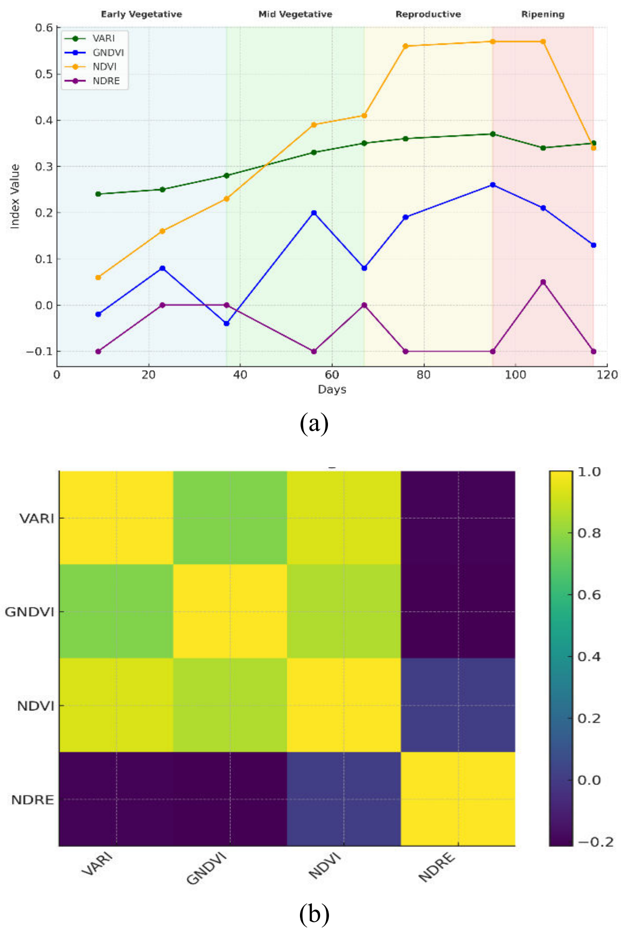

Figure-14. (a) Time series of VARI, GNDVI, NDVI, and NDRE, and (b) Correlation matrix of relationships among VARI, GNDVI, NDVI, and NDRE.

 ISSN 1819-6608
ARPN Journal of Engineering and Applied Sciences

CONCLUSIONS

In this study, we developed a technique for extracting detailed information on rice growth characteristics using high-resolution aerial imagery. Over the course of the study, nine series of aerial images were acquired periodically from day 9 to day 117 of rice growth. These images were processed to generate digital products, which were then used to derive key vegetation indices for analyzing rice growth stages. The effectiveness of the spectral feature extraction technique was validated through the application of multispectral aerial image processing algorithms. These algorithms successfully extracted plant spectral features, reflecting the various rice growth stages through the derivation of the Visible Atmospherically Resistant Index (VARI), Green Normalized Difference Vegetation Index (GNDVI), Normalized Difference Vegetation Index (NDVI), and Normalized Difference Red Edge Index (NDRE). Correlation analysis reveals strong relationships between NDVI and VARI ($r \approx 0.93$), NDVI and GNDVI ($r \approx 0.88$), and VARI and GNDVI ($r \approx 0.78$), indicating that these indices capture similar trends in canopy development. NDRE, however, exhibits weak or negligible correlation with the others (r = -0.20 to 0.15), suggesting that it captures complementary information not captured in visible-spectrum indices.

ACKNOWLEDGEMENTS

The authors would like to thank the Malaysian Ministry of Higher Education (MOHE) for funding this research through the Universiti Teknikal Malaysia Melaka (UTeM) Research Matching Grant (INDUSTRI (URMG)/ANJUNG/2024/FTMK/I00092) and for all the support throughout this research.

REFERENCES

[1] Tengli M. B., O. P. Sharma. 2017. Strategies to Overcome Constraints in the Adoption of Improved Paddy Cultivation Practices in Navsari and Surat Districts of South Gujarat, India. International Journal of Current Microbiology and Applied Sciences. 6(11): 932-937.

[2] Khazanah Research Institute. 2019. The Status of the Paddy and Rice Industry in Malaysia. Khazanah Research Institute, Kuala Lumpur, Malaysia.

[3] Gerten D., V. Heck, J. Jägermeyr. 2020. Feeding Ten Billion People is Possible within Four Terrestrial Planetary Boundaries. Nature Sustainability. 3: 200–208.

[4] Meng L., Y. Li, R. Shen, Y. Zheng, B. Pan, W. Yuan, J. Li, L. Zhuo. 2024. Large-Scale and High-Resolution Paddy Rice Intensity Mapping Using Downscaling and Phenology-Based Algorithms on Google Earth Engine. International Journal of Applied Earth Observation and Geoinformation. 128: 1-19.

[5] Sufahani S., M. G. Kamardan, M. S. Rusiman, M. Mohamad, K. Khalid, M. Ali, K. Khalid, M. K. M. Nawawi, A. Ahmad. 2018. A Mathematical Study on the Additive Technique versus the Branch and Bound Technique for Solving the Binary Programming Problem. Journal of Physics: Conference Series. 995(1): 012001.

[6] Eng L. S., R. Ismail, W. Hashim, A. Baharum. 2019. The Use of VARI, GLI, and VIgreen Formulas in Detecting Vegetation in Aerial Images. International Journal of Technology. 10(7): 1385-1394.

[7] Subramaniam M., R. Yogambigai, R. Khalid. 2017. Estimation of Future Paddy Production and Sustainable Land Allocation in Malaysia: A Polynomial Approach. Pertanika Journal of Social Science and Humanities. 25: 1613-1624.

[8] Fellmann T., P. Witzke, F. Weiss. 2018. Major Challenges of Integrating Agriculture into Climate Change Mitigation Policy Frameworks. Mitigation and Adaptation Strategies for Global Change. 23: 451-468.

[9] Weiss M., F. Jacob, G. Duveiller. 2020. Remote Sensing for Agricultural Applications: A Meta-Review. Remote Sensing of Environment. 236: 1-19.

[10] Ahmad A., H. Sakidin, M. Y. A. Sari, A. R. M. Amin, S. F. Sufahani, A. W. Rasib. 2021. Naïve Bayes Classification of High-Resolution Aerial Imagery. (IJACSA) International Journal of Advanced Computer Science and Applications. 12(11): 168-177.

[11] www.knowledgebank.irri.org. 2022. Crop Calendar - IRRI Rice Knowledge Bank. Available at: http://www.knowledgebank.irri.org/images/stories/crop-calendar-growth-tpr.jpg [Accessed 24 Sep. 2022].

[12] Wu W., L. Yang, X. Liao, B. Deng, B. Zhao. 2020. A Smart Agriculture System Design Based on Edge Computing. IEEE Access. 8: 101484-101494.

[13] Maimaitijiang M., R. Sagan, S. Sidike, M. Hartling, F.M. Esposito, B. Fritschi, L. Maimaitiyiming, J. Newcomb, A. Layton, A. Pitesky, *et al.* 2020. Soybean Yield Prediction from UAV Using

Multitemporal and Multisensor Data Fusion and Deep Learning. Remote Sensing of Environment. 237: 1-15.

[14] Yuan J., T. Ren, T. Wang, Z. Lu. 2020. Rice Yield Estimation Using UAV-Based Hyperspectral Images and Machine Learning Algorithms. Remote Sensing. 12(4): 1-17.

[15] Caballero R. J., C. F. Sirmacek. 2021. Rice Plant Health Assessment Using UAV-Based RGB Imagery and Machine Learning. Precision Agriculture. 22(1): 110-130.

[16] Rizwan M., M. Awais, A. Ahmad, M. Zahoor, A. Latif. 2022. CNN-Based Image Classification for Paddy Disease Detection. Computers, Materials & Continua. 73(1): 1365-1381.

[17] Nuwan M., R. Gamage, M. Bandara. 2020. Rice Growth Stage Detection Using UAV Imagery and Deep Learning Techniques. Agricultural Informatics. 11(1): 28-35.

[18] Singh V., A. Jain. 2019. A Deep Learning-Based Approach for the Detection of Pest Infestation in Rice Crops. Artificial Intelligence in Agriculture. 1(2): 45-52.

[19] Cheng Y., X. Hu, Y. Meng, H. Wang. 2021. Automated Rice Disease Diagnosis Using a Novel Hybrid CNN Model. Computers and Electronics in Agriculture. 187: 106252.

[20] Masjuki H. H., M. A. Kalam, M. Zulkifli, A. M. Ashraful, S. M. Mahmudul, F. Risaldi. 2016. Renewable and Sustainable Biofuel Production from Palm Oil-Based Feedstock. Energy Conversion and Management. 126: 534-547.

[21] Zhang Y., L. Zhang, S. Wu, J. Li. 2020. Combining Remote Sensing and Crop Growth Models for Rice Yield Estimation: A Review. Sensors. 20(23): 1-25.

[22] Ahmad A. 2012. Classification Simulation of the RazakSAT Satellite. Procedia Engineering. 53: 472-482.

[23] Hasan M. M., R. Mahmud, M. S. Islam, M. A. Rahman. 2021. Monitoring Rice Crop Growth Using Sentinel-2 and Machine Learning Techniques. Agriculture. 11(8): 737.

[24] Ahmad A., B. M. Aboobaider, M. S. M. Isa, S. Muhamad, S. Man. 2014. Temporal Changes in Urban Green Space Based on Normalized Difference Vegetation Index. Applied Mathematical Sciences. 8(53-56): 2743-2751.

[25] Lima I., G. Romeu, P. de Lima, João. 2021. Remote Sensing Monitoring of Rice Fields: Towards Assessing Water Saving Irrigation Management Practices. Frontiers in Remote Sensing. 2: 1-13.

[26] Asawapaisankul R., Rattanapichai W., Sajjaphan K., Pitakdantham R., Sermsak R., Lukas V., Klem K., & Tubana B. 2025. Correlation of yield and vegetation indices from unmanned aerial vehicle multispectral imagery in Thailand rice production systems. Agrosystems, Geosciences & Environment. 8: 1-12.

[27] Ahmad A., S. Quegan. 2014. Multitemporal Cloud Detection and Masking Using MODIS Data. Applied Mathematical Sciences. 8(7): 345-353.

[28] Ahmad A., S. Quegan. 2014. Haze Modelling and Simulation in Remote Sensing Satellite Data. Applied Mathematical Sciences. 8(157-160): 7909-7921.

[29] Ahmad A., M. K. Abdul Ghani, S. Razali, H. Sakidin, N. Md Hashim. 2014. Haze Reduction from Remotely Sensed Data. Applied Mathematical Sciences. 8(33-36): 1755-1762.